Evaluation of the Lagrangian Particle Model GRAL against the US-EPA near Roadway Tracer Study 2008

D. Oettl

Air Quality Control, Government of Styria, Graz, Styria, 8010, Austria, Dietmar.oettl@stmk.gv.at

Keywords: GRAL, dispersion modelling, microscale flow field, noise abatement wall, NRTS 2008

Abstract

A refined microscale flow field model has been implemented in the Lagrangian Particle Model GRAL (Graz Lagrangian Model) to provide flow fields for the dispersion module. The flow field model is based on the Reynolds-averaged Navier-Stokes equations (RANS) and uses a standard k-ε turbulence model. In this work, the whole model was tested against the comprehensive Near Roadway Tracer Study (NRTS 2008) conducted by the US-EPA. The experiment comprised well defined tracer releases from a line source and corresponding tracer concentrations with and without a mock sound barrier in flat terrain. In addition, an array of sonic anemometers provided not only mean wind speeds and –directions but also turbulence quantities like turbulent kinetic energy or three-dimensional wind speed variances. It became evident, that GRAL in its current version (still with research status and not an official release) is in principle able to provide reasonable tracer concentrations for both non-barrier and barrier sampling grids. In case of the non-barrier experiments, GRAL performs somewhat better than Gaussian-type line source models with respect to average as well as peak concentrations, but gives less good results when taking normalised mean square error as quality indicator. However, there are some significant differences between observed and modelled turbulent kinetic energy and wind speed profiles in the wake region of the barrier, which might be triggered by inconsistent formulations for inflow profiles of turbulent kinetic energy and average turbulent dissipation rates in general in GRAL.

Introduction

In Austria, Lagrangian Particle Models become increasingly popular for regulatory applications. The majority of cases have to deal in one way or another with the influence of buildings on the pollutant or odour dispersion. Some models, such as the German standard model AUSTAL2000 (Janicke, 2014), make use of microscale diagnostic wind field models to take such effects into account. While diagnostic wind field models require little computation time, they are not able to provide reliable flow fields in complex build-up areas.

Thus, attempts have been undertaken to implement a prognostic, non-hydrostatic, microscale wind field model in the Lagrangian particle model GRAL (Oettl, 2013) with emphasis to keep computational times low to enable regulatory applications. Herein, the current status of the wind field model and numerical methods are described, as well as first evaluation results using an extensive field experiment carried out by the US-EPA (Finn et al., 2010) in 2008. Apart from the computed flow fields, also modelled tracer concentrations were compared with observations.

The field experiment (Near Roadway Tracer Study, NRTS 2008) aimed at studying the effects on concentrations of roadway emissions behind a roadside sound barrier in various conditions of atmospheric stability. Supporting measurements of meteorology were performed by an array of 6 sonic anemometers employed at the up- and downwind sides of the barrier, which allow for testing models with respect to computed mean flow and turbulence fields.

Currently, GRAL is also tested against flow field observations from several wind tunnel experiments taken at the large boundary-layer wind tunnel of the University of Hamburg (Grawe et al. 2014). These are not yet finished, and will be published in the near future. Therefore, results presented in this paper are not those of the actual official release of GRAL (Version 13.3.), but have to be considered as intermediate ones with a research version of GRAL. As soon as all evaluation steps of the entire quality assurance of GRAL have been accomplished, the research version will turn to an official release. Apart from additional field and wind tunnel experiments, used for model evaluation (Oettl, 2013), GRAL is also intensively tested over a couple of months in practical applications prior to any official release.

Model description

The microscale flow field model is based on the well-known Reynolds-averaged Navier-Stokes equations (RANS), neglecting molecular viscosity, Coriolis and buoyancy forces, and utilizing an eddy viscosity turbulence model:

$$\frac{\partial \overline{u_i}}{\partial t} + \overline{u_j}\frac{\partial \overline{u_i}}{\partial x_j} = -\frac{1}{\rho}\frac{\partial \overline{p}}{\partial x_i} + \frac{\partial}{\partial x_j}\left[K\left(\frac{\partial \overline{u_i}}{\partial x_j} + \frac{\partial \overline{u_j}}{\partial x_i}\right) - \frac{2}{3}\delta_{ij}k\right] \quad (1)$$

$\overline{u_i}$ mean wind speed in horizontal and vertical directions

ρ air density

$\frac{\partial \overline{p}}{\partial x_i}$ mean pressure gradient acceleration

k, ε turbulent kinetic energy, and dissipation rate

K eddy viscosity

The eddy viscosity is computed via

$$K = 0.09 \cdot \sqrt{k} \cdot x_3, \quad (2)$$

and the standard *k-ε* turbulence model (e.g. Rodi, 1980):

$$\frac{\partial k}{\partial t} + \frac{\partial \overline{u_j} k}{\partial x_j} = \frac{\partial}{\partial x_j}\left(K\frac{\partial k}{\partial x_j}\right) + P_m + P_b - \varepsilon \quad (3)$$

$$\frac{\partial \varepsilon}{\partial t} + \frac{\partial \overline{u_j}\varepsilon}{\partial x_j} = \frac{\partial}{\partial x_j}K\left(\frac{\partial \varepsilon}{\partial x_j}\right) + \frac{\varepsilon}{k}\left(1.44 \cdot \left(P_m + P_b\right) - 1.92 \cdot \varepsilon\right) \quad (4)$$

P_m Production term for turbulent kinetic energy due to shear stresses

P_b Production term for turbulent kinetic energy due to buoyancy

$$P_m = K \cdot \left(\frac{\partial \overline{u_i}}{\partial x_j} + \frac{\partial \overline{u_j}}{\partial x_i}\right) \cdot \frac{\partial \overline{u_i}}{\partial x_j} \quad (5)$$

$$P_b = 1.35 \cdot K \cdot \frac{g}{\theta_0}\frac{\partial \overline{\theta}}{\partial x_3} \quad (6)$$

Equation (2) was chosen instead of $K = 0.09 \cdot \frac{k^2}{\varepsilon} \cdot$ because results appeared to be a bit less grid size dependent, which is one crucial necessity to comply with the VDI guideline 3783-9 (2005).

The temperature gradient $\frac{\partial \overline{\theta}}{\partial x_3}$ is a function of stability class, and is kept constant throughout a simulation. Conservation of mass is obtained by solving the Poisson equation after each time step:

$$\rho \frac{\partial \overline{u_i}}{\partial x_i} = \frac{\partial^2 \overline{p}}{\partial x_i^2} dt \,, \tag{7}$$

At the lowest grid cell and next to building surfaces *k* and *ε* are computed diagnostically (Eichhorn, 2011):

$$k = \frac{u_*^2}{\sqrt{c_\mu}} \tag{8}$$

$$\varepsilon = \frac{u_*^3}{\kappa z_1} \tag{9}$$

$c_\mu = 0.09$, $\kappa = 0.4$, u_* = friction velocity, and z_1 = cell height of first cell above ground or obstacles.

Surface friction is taken into account by adding the following source term in the discretised conservation equations for momentum at the first layer above ground:

$$-\frac{\overline{u_i}}{\overline{v}_1} \cdot u_*^2 \cdot \Delta x \cdot \Delta y \tag{10}$$

$\overline{v}_1$ mean wind speed in the first layer

In order to solve the conservation equations numerically, a finite volume method utilizing a stagger grid is applied as drawn in **Figure 1** for one dimension. ϕ stands for any conserved quantity, such as turbulent kinetic energy, or dissipation rate, while u_w is the transport velocity over the western cell face. Non-hydrostatic pressure is also located in the centre of each grid cell (ϕ_P), and transport velocities u_w and u_e are corrected (eq. 7) after each time step to match mass conservation. Up to this point, the method of Patankar (1980) is followed. However, he suggested solving the momentum equations for each u_w separately. This would mean to solve subsequently three momentum equations in each space direction, and afterwards equations for k and ε. To speed up the numerical integration, it is desirable to solve all conservation equations in one loop over all grid cells, instead of subsequent loops. Hence, in GRAL, together with k and ε, also the conservation equation for momentum is solved for the wind speed components, defined in the centre of a grid cell and taken as average over the two neighbouring values at the cell faces (u_w and u_e). Averaging is done immediately after the pressure correction for the velocities at the cell faces (u_w and u_e) has been carried out. This simple re-adjustment of the originally proposed integration method of Patankar (1980) considerably speeds up the simulations, while still avoiding the problem of decoupling between pressure correction and momentum equations. One disadvantage is that the pressure force in the momentum equations $-\frac{1}{\rho}\frac{\partial \overline{p}}{\partial x_i}$ has to be computed over two neighbouring grid points (p_w and p_e) and is thus, somewhat smoothed. Comparisons with the original method proposed by Patankar (1980) neither showed significant differences in the resulting flow fields, nor were numerical instabilities observed over the bulk of test cases already used for model evaluation.

Conservation equations are solved by a fully implicit time discretization scheme, and the “power law” method suggested by Patankar (1980). For the west face of a grid cell with a volume $\Delta x \Delta y \Delta z$ it can be written as (using the notation of Patankar):

$$a_W = D_w \cdot \max\left[0, \left(1 - \frac{0.1|F_w|}{D_w}\right)^5\right] + \max\left[0, F_w\right] \tag{11}$$

$$D_w = \rho K \frac{\Delta y \Delta z}{\Delta x} \text{, and } F_w = \rho u_w \Delta y \Delta z \quad (12)$$

The reader is referred to Patankar (1980) for detailed information about all other terms appearing in the fully implicit time discretization equation of any quantity ϕ (here for simplicity written in one dimension):

$$a_P \phi_P = a_E \phi_E + a_W \phi_W + b \quad (13)$$

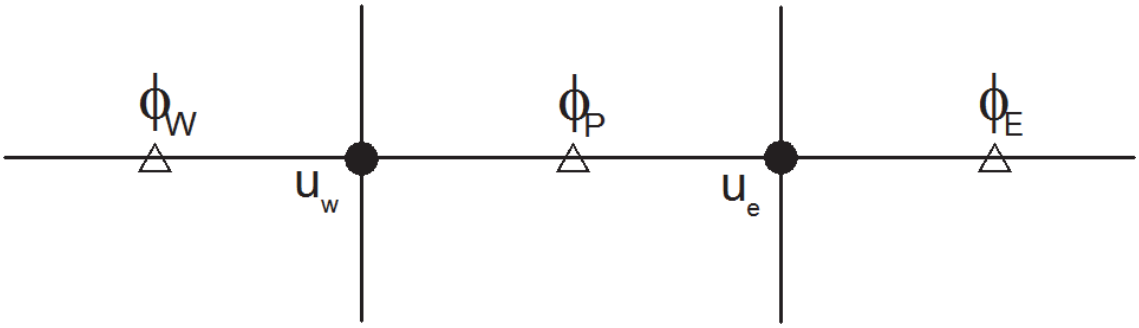

Figure 1: Grid used in GRAL to discretise conservation quantities

Finally, the flow is computed by an iterative procedure following the SIMPLE (Semi-Implicit Method for Pressure Linked Equations) algorithm of Patankar (1980) in a slightly modified form:

1. First guess wind field (one dimensional vertical profile, horizontally homogenous)
2. Dirichlet lateral boundary conditions at inflow boundaries and homogenous Neumann boundary conditions at outflow faces for velocities. Inside buildings velocities are set zero.
3. Mass divergence for each cell volume
4. Poisson equation (new pressure field)
5. Pressure correction of velocities at cell faces. Updated pressure gradients for the RANS equations are obtained by computing pressure gradients from the new pressure field and adding these to the pressure gradient of the previous time step. In a converged solution the new pressure field becomes zero. No under-relaxation is applied.
6. New averaged velocities at cell centres
7. Conservation equations for momentum, turbulent kinetic energy, and dissipation using a tri-diagonal-matrix algorithm (TDMA)
8. New uncorrected velocities at cell faces by linear interpolation between velocities obtained at cell centres
9. Return to point 2

As stated in the introduction, GRAL is mainly used in applications for regulatory purposes. Thus, computation times need to be small enough to enable operation on conventional PCs or Laptops. For larger domains of some hundreds of metres up to a few kilometres, and grid sizes below 5 m, CFD simulations can be quite demanding. In order to make use of multiple CPUs, GRAL has been parallelized introducing OpenMP statements in the Fortran code. Furthermore, the microscale wind field model is only applied in regions around buildings up to 15 times the building heights. While horizontally only constant grid spacing is allowed in the current version, a user may define a stretching factor ≥ 1.0 vertically to save computation time. GRAL is mostly used by non-specialists in CFD modelling, which limits the number of parameters provided for users typically provided by such models to make sure results are numerically stable and represent steady-state conditions (e.g. relaxations factors, time step policy). Currently, a user can only adjust the simulation grid, thus, all other parameters are set automatically in GRAL.

Simulations in this work were performed using the newly implemented steady-state condition, which was derived on the bases of comprehensive wind tunnel tests provided by the German Guideline VDI 3783-9 (2005) on quality assurance of microscale prognostic wind field models. It uses a lower limit for the normalised non-hydrostatic pressure correction of 0.1 (averaged over 100 subsequent time steps). Normalisation is done by $\rho \cdot \bar{v}_{top}{}^2$, where $\bar{v}_{top}$ is the wind speed at the top of the model domain.

Another important issue for practical applications is the necessity that meteorological input data can easily be derived from routine observational networks. Although it is possible to use vertical profiles of measured mean wind- and turbulence quantities in GRAL, the most widespread method for initializing the model is using solely mean wind speeds, and -directions at a certain height, and stability classes. The recommended method to derive stability classes for GRAL as well as the meteorological pre-processor to gain values for friction velocity, Obukhov length, and boundary-layer-height, from this simple input data, is outlined in Oettl (2013). From these scaling parameters, standard profiles for dissipation rate, and standard deviations of wind velocity fluctuations σ_i are calculated. In turn, these standard profiles are used to define lateral boundary conditions and initial values for turbulent kinetic energy and dissipation rate for the microscale flow field model, too.

A detailed description of the dispersion module of GRAL would be go beyond the scope of this work. Readers are referred to the elaborate model documentation given in Oettl (2013).

Experimental data set (Finn et al., 2010)

In October 2008 the US-EPA conducted several tracer experiments to investigate the flow and dispersion with and without a 6 m high and 90 m long sound barrier, made of straw bales. As emission source, a 54 m long line source was set up at a distance 6 m upwind of the barrier. Tracer was released simultaneously at two grids, separated by a distance of about 700 m, being completely identical regarding source and receptor points (**Figure 2**), except at one site there was no barrier.

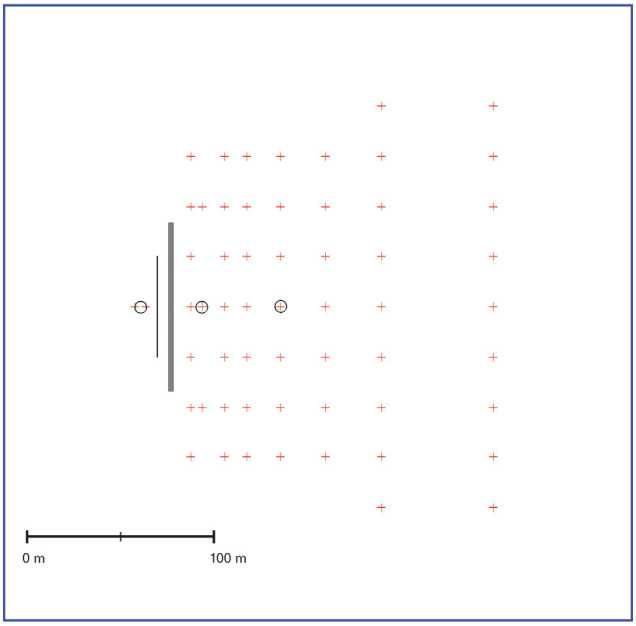

Figure 2: Sketch of the experimental layout for the site with sound barrier. Crosses indicate tracer sampling points, circles the positions of sonic anemometers, the sound barrier is drawn in grey, the line source in black, and the rectangle marks the model domain of GRAL.

Each tracer release lasted 3 hours and sampling took place over an averaging period of 15 minutes. All in all 5 releases were carried out in different meteorological conditions, characterised by quite distinct observed mean wind speeds and stabilities (**Table 1**). During exp. 4 wind directions were mostly from the wrong sector, thus it was decided not to use it in this study. In exp. 1 neutral atmospheric stabilities prevailed, and high wind speeds were observed. Exp. 2 in contrast was carried out during convective, low wind speed conditions, while moderate wind speeds and slightly stable conditions were measured in exp. 3. Finally, experiments 4 and 5 where influenced by low wind speeds and very stable layering of the atmosphere, leading to the highest tracer concentrations.

Table 1: Observed mean inverse Monin-Obukhov length, wind speed and -direction for the tracer experiments at the site without barrier

Exp.	sampling points w/o barrier	wind speed [m/s]	wind direction [deg.]	z/L [-]
1	654 / 640	6.7	266	-0.014
2	676 / 685	1.4	238	-0.34
3	680 / 685	3.1	276	0.10
4	336 / 345	1.5	127	0.32
5	587 / 679	1.8	284	0.28

The measurements comprised also wind observations utilizing sonic anemometers at the following locations:

Table 2: Locations of sonic anemometers at the experimental site with a 6 m high barrier (H=Height of the barrier)

Sonic	X (m)	Y (m)	Z (m)
A	-1.6 H	0	3
B	4 H	0	3
C	4 H	0	6
G	4 H	0	9
D	11 H	0	3

The experimental site is located across a broad, relatively flat plain with low lying scrubs. An average roughness length of 0.05 m is obtained when applying the idealized logarithmic wind profile law for neutral stability to sonic data observed 3 m above ground level at the non-barrier site in experiment 1.

$$\bar{v}(x_3) = \frac{u_*}{\kappa} \ln\left(\frac{x_a}{z_0}\right) \tag{14}$$

In stable conditions one might use (Venkatram and Du, 1997)

$$\bar{v}(x_3) = \frac{u_*}{k} \cdot \left[\ln\left(\frac{x_a}{z_0}\right) + 5 \cdot \left(\frac{x_a}{L}\right)^2\right] \tag{15}$$

for instance, to derive roughness lengths accordingly. Using sonic data from exp. 5 gives an average roughness length of 0.03 m. In both equations x_a is the anemometer height above ground level and κ the Von Karman constant (0.4 was taken in this analysis).

Apart from the roughness length, GRAL was driven by observed wind speeds, and –directions upwind of the barrier (sonic A). Instead of using locally measured turbulence data from the sonic anemometers, stability classes were estimated according to the modified US-EPA (2000) method as outlined in Oettl (2013) and used to derive all necessary turbulence quantities needed in the Lagrangian Particle Model. The corresponding meteorological pre-processor is described in detail in Oettl (2013). The motivation to do so is based on the circumstance that this is the usual way to operate GRAL in applications for regulatory purposes, and the model should be evaluated in an operation mode as close as possible as in everyday business. Meteorological input was the same for the barrier and non-barrier grid simulations.

In each run 540,000 particles were released from the source, and horizontal resolution used for the flow field modelling and concentration grid was 2 m, and 1 m in the vertical.

Results

As has already been found in previous investigations (e.g. Hagler et al., 2011; Heist et al., 2009; Esser 1985; Romberg 1988; Hoelscher et al., 1993; Bowker et al., 2007; Okamoto et al., 1999; Oettl et al., 2003) sound barriers lead in general to lower concentrations at the downwind side but increased concentrations at the upwind, on-road side. When considering the ratios of mean observed concentrations at receptor points downwind of the barrier (only those receptors between -4.5H and

+4.5H in crosswind direction were used) and corresponding ones without barrier for the four experiments discussed herein, a reduction for this experimental layout of about 80 % is evident (**Table 3**). GRAL has a tendency to slightly overestimate the barrier effect but still is in good agreement with observations. It seems as if the barrier effect is more pronounced in low wind speed conditions, as can be seen from observed as well as modelled ratios.

The rather strong concentration reduction effect of the sound barrier in the NRTS 2008 experiment should not be taken granted in general, for traffic induced turbulence was utterly absent. Such generates an emission zone with a vertical extension of some metres, while the line source set up in the NRTS experiment extents merely more than a few centimetres. For instance, Steffens et al. (2013) used a distance of 0.25 m in x- and z-directions to define the line source of this experiment in their modelling study.

Table 3: Ratio of observed and modelled mean receptor concentrations downwind of the sound barrier and mean corresponding concentrations at the non-barrier grid

Exp.	Ratio	
	Obs.	Mod.
1	0.29	0.22
2	0.19	0.16
3	0.25	0.22
5	0.17	0.13
Mean	0.23	0.18

There are many statistical measures discussed in literature, which can serve as indicator for model performance. For example, the normalised mean square error (NMSE) is often used, because it allows for data set independent comparison of model results (ASTM, 2000). The disadvantage of the NMSE is the fact that possible over- or underestimations can't be assessed. Thus, in the following also the fractional bias FB is utilized as additional performance indicator.

$$FB = \frac{\left(\overline{c}_o - \overline{c}_p\right)}{0.5 \cdot \left(\overline{c}_o + \overline{c}_p\right)} \tag{16}$$

$$NMSE = \frac{\overline{\left(c_o - c_p\right)^2}}{\overline{c}_o \cdot \overline{c}_p} \tag{17}$$

Table 4 lists both statistical measures for each experiment and all data points. Chang and Hanna (2004) suggested using an upper bound for the NMSE < 4, and a maximum of 0.3 for the $\left|FB\right|$ as criteria to define acceptable model performance. In most experiments these criteria are met and it can be seen, that GRAL performs quite similar concerning all data points for the barrier and non-barrier experiments. Stocker et al. (2013) presented results for the non-barrier grid for some Gaussian type line source models (ADMS-Roads, CALINE4, AERMOD, RLINE). Concerning the NMSE, although simpler in physics than GRAL, these models perform better than GRAL. NMSE values ranged between 0.96 and 1.97, while values for the FB – ranging between -0.22 and -0.42, are higher than those obtained with GRAL, and except for the model RLINE, which was developed on the basis of the NRTS 2008, did not fulfil the criteria proposed by Chang and Hanna (2004). It can be concluded that in the simpler case without barrier, simpler and thus much faster Gaussian type models are of equal quality than GRAL. One may anticipate, though, in more complex situations, like in the presence of sound walls, more sophisticated models solving e.g. RANS equations are superior.

Figure 3 depicts quantile-quantile plots of observed and modelled concentrations for the non-barrier and barrier grids. As data points are well aligned along the ideal 1:1 line with little scatter, GRAL obviously performs rather well with this respect. Interestingly, even peak concentrations are captured well. In contrast, results published by Stocker et al. (2013) for ADMS-Roads and RLINE indicate a significant underestimation of peak concentrations for the NRTS 2008 without sound barrier.

Table 4: Performance indicators for GRAL

Exp.	barrier grid		non - barrier grid	
	FB	NMSE	FB	NMSE
1	0.3	0.7	0.0	0.1
2	-0.3	2.4	-0.2	4.8
3	-0.1	2.3	-0.2	0.7
5	0.3	1.9	0.1	2.0
All	0.1	3.7	0.0	3.2

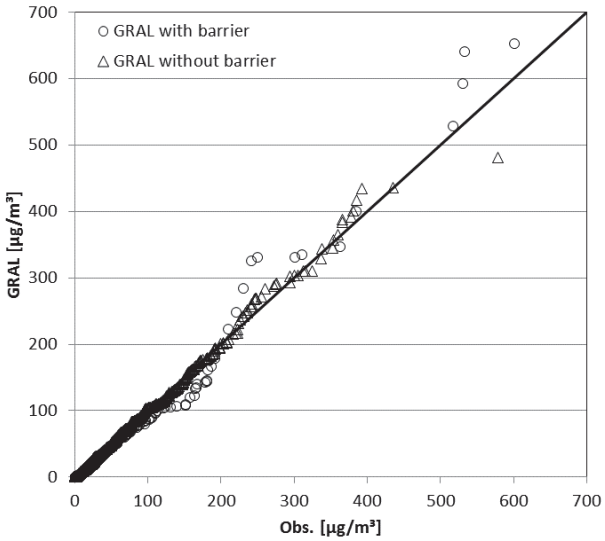

Figure 3: Quantile-quantile plot of observed and modelled concentrations with and without sound barrier

The extensive wind and turbulence measurements during the NRTS 2008 allow for additional testing of microscale flow models, too. Such an investigation has been performed by Steffens et al. (2013) recently, who compared results obtained with a RANS and a LES model. They found that the LES turbulence model was more accurate in overall.

Sonic anemometers A (-1.1H, 3 m) and D (11H, 3 m) measured nearly the same average wind speeds, though, observed TKE at anemometer D is about double the one at sonic A. Regarding wind speed GRAL is in quite good agreement with observations at these sites, while modelled TKE are underestimated by about a factor of two for both locations. Interestingly, also GRAL suggests an average TKE at site D double the value at site A.

The recirculation induced by the mock sound barrier with a height of 6 m can nicely be seen at sonic sites B, C, and E, which were placed at a downwind distance of 4 H from the obstacle (see **Figure 4** and **Figure 5**). The minimum of observed wind speeds is visible at 6 m height, which is quite interesting, because observations in wind tunnel experiments typically indicate minimum wind speeds somewhere around 0.5 H within recirculation zones. GRAL is not able to capture this indeed surprising observation, but shows a slight increase in wind speed between 3 m and 6 m height.

Also, contrasting RANS simulations showing usually a peak in modelled TKE at around 1 (e.g. Olesen et al., 2009)Along wind speeds in the recirculation zone as simulated with GRAL are - in their tendency to increase with height - in agreement with observations, but GRAL does not reproduce backward flows 3 m above ground level as evident from the measurements (**Figure 5**). Wind tunnel investigations for a quasi-two-dimensional barrier, as reported in Grawe et al. (2013), resulted in maximum wake regions of 4-5 H. In the case of the NRTS 2008 it is obvious, that the recirculation zone extends even farther, which might be caused by the lower surface roughness of ~0.03 m compared with the roughness in the cited wind tunnel experiment of 0.10 m. Though, Grawe et al. (2013) conducted also simulations with their model MITRAS for the same configuration of a quasi-two-dimensional barrier with smaller roughness length of 0.03 m, which resulted in an increase of the wake

region by only about 25 %. Still it seems as if there exist major differences in the boundary-layers generated by wind tunnels and those in reality. Note, that the negative along-wind components were found in all experiments on average, independent on stability and wind speed at site B.

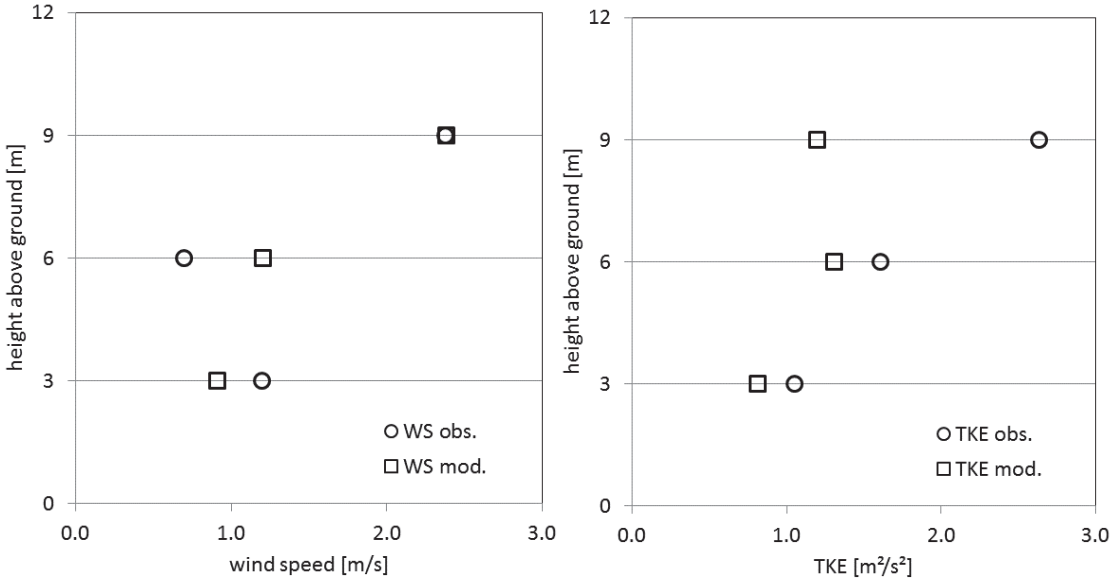

Figure 4: Observed and modelled average wind speeds and turbulent kinetic energy at 4H downwind distance from the barrier

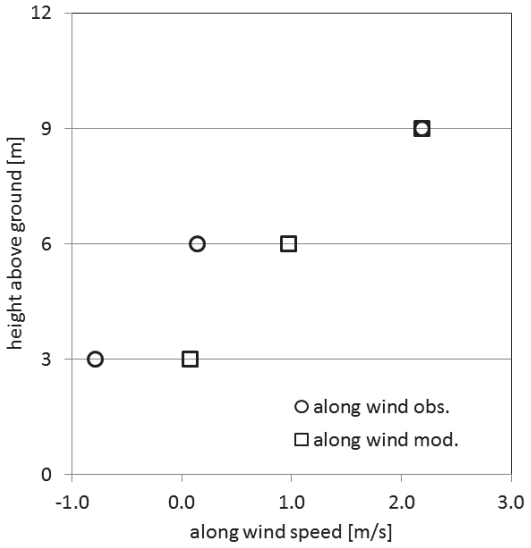

Figure 5. Observed and modelled average along wind speeds at 4H downwind distance from the barrier

Conclusions

The implementation of a refined RANS based microscale flow field model, using the standard *k-ε* turbulence model, in the Lagrangian Particle Model GRAL improves simulation results in applications, where obstacles influence pollutant dispersion. Still model development is not finalised, due to further necessary evaluations being part of the overall quality assurance as documented in Oettl (2013).

Particularly, this study brought evidence of some deficiencies of GRAL with respect to modelled flows behind a mock sound barrier as observed during the NRTS 2008. On the other hand, GRAL already gives quite satisfying results (not published yet) when compared with comprehensive wind tunnel data as required by the German guideline VDI 3783-9 (VDI, 2005). The reason might be an inadequate formulation of inlet boundary conditions for turbulent kinetic energy and dissipation as discussed for instance in the publication of Parente et al. (2011). Linking prognostic microscale flow field models

closely with Lagrangian Particle Models is in general a very promising approach, which provides a wide field of model applications. Due to the advances in computer technology, GRAL is already applicable for regulatory purposes. Computation times for the complete NRTS 2008 experiments were less than one hour on modern PCs.

References

ASTM, 2000. Standard guide for statistic evaluation of atmospheric dispersion model perfomrance. American Society for Testing and Materials, Destination D 6589-00 ASTM Internatinoal, West Conshohocken, PA (USA), 17 pp

Bowker, G. E., Baldauf, R., Isakov, V., Khlystov, A., Petersen, W. (2007): The effects of roadside structures on the transport and dispersion of ultrafine particles from highways. *Atmospheric Environment*, 41 (37), 8128-8139.

Chang, J.C., and S.R. Hanna (2004): Air quality model performance evaluation. *Met and Atmos Physics*, 87, 167-196

Eichhorn, J. (2011): MISKAM. Handbuch zu Version 6. pp 60. URL: http://www.lohmeyer.de/de/system/files/content/download/software/HB_MISKAM.pdf

Esser J (1985): On the influence of copse and noise barriers on the pollutant dispersion near road ways (German). Straßenverkehrstechnik, 29: 90–94

Finn, D., Clawson, K.L., Carter, R.G., Rich, J.D., Eckman, R.M., Perry, S.G., Isakov, V. and Heist, D.K. (2010): Tracer studies to characterize the effects of roadside noise barriers on near-road pollutant dispersion under varying atmospheric stability conditions. *Atmos. Environ.*, **44**, 204-214.

Grawe, D., W. Bächlin, H. Brünger, J. Eichhorn, J. Franke, B. Leitl, W. J. Müller, D. Oettl, M. Salim, K. H. Schlünzen, Ch. Winkler, and M. Zimmer (2014): An updated evaluation guideline for prognostic microscale wind field models. 6th Int. Symposium on Computational Wind Engineering, 8 – 12. June Hamburg.

Grawe, D., K. H. Schlünzen, F. Pascheke (2013): Comparison of results of an obstacle resolving microscale model with wind tunnel data. Atmospheric Environment, 79, 495-509

Hagler, G. S., W. Tang, M. I. Freeman, D. K. Heist, S. G. Perry, A. F. Vette (2011): Model evaluation of roadside barrier impact on near-road air pollution. Atmospheric Environment, 45 (15), 2522-2530.

Heist, D. K., S. G. Perry, L. A. Brixey (2009): A wind tunnel study of the effect of roadway configurations on the dispersion of traffic-related pollution. Atmospheric Environment, 43, 5101-5111.

Hoelscher, N., Höffer, R., Niemann, H.J., Brilon, W., Romberg, E. (1993): Wind tunnel experiments on micro-scale dispersion of exhausts from motorways. *The Science of the Total Environment* 134, 71-79

Janicke, U., 2014. AUSTAL2000. Program Documentation of Version 2.6. Federal Environmental Agency, Dessau-Roßlau (Germany), Janicke Consulting, Überlingen (Germany), pp 123. URL: http://www.austal2000.de/data/2014-02-27/austal2000_en.pdf

Oettl, D., R. A. Almbauer, P. J. Sturm, and G. Pretterhofer (2003): Dispersion modelling of air pollution caused by road traffic using a Markov Chain - Monte Carlo model. *Stochastic Environmental Research and Risk Assessment*, 58-75.

Oettl, D. (2013): Documentation of the Lagrangian Particle Model GRAL 13.3. Amt d. Stmk. Landesreg., Referat für Luftreinhaltung. Ber.Nr. LU-03-13, 116 pp.

Oettl, D., A. Goulart, G. Degrazia, D. Anfossi (2005): A new hypothesis on meandering atmospheric flows in low wind speed conditions. *Atmos. Environ.*, **39**, 1739 – 1748.

Okamoto S, Ohnshi H, Yamada T, Itohiya T (1999): A database for highway air quality modeling. Proceedings of the 8th International Symposium on Transport and Air Pollution, P. Sturm (Ed.), Graz (Austria), 541–548

Olesen, H. R., R. Berkowicz, M. Ketzel, P. Løfstrøm (2009): Validation of OML, AERMOD/PRIME and MISKAM using the Thompson Wind-Tunnel Dataset for Simple Stack-Building Configurations. *Bound.-Layer Meteorol*, 131: 73-83

Parente, A., C. Gorlé, J. van Beeck, C. Benocci (2011): A comprehensive modelling approach for the neutral atmospheric boundary layer: consistent inflow conditions, wall function and turbulence model closure. Boundary-Layer Meteorology, 140 (3), 411-428

Patankar S.V. (1980): Numerical Heat Transfer and Fluid Flow. Mc-Graw-Hill Book Company, New York, pp. 197, ISBN: 0-89116-522-3.

Rodi, W. (1980): Turbulence Models and Their Application in Hydraulics - A State of the Art Review. Iahr Monograph Series, A. A. Balkema, Delft.

Romberg E (1988): Wind tunnel studies on the influence of traffic, copse, and noise barriers on the dispersion of pollutants near streets (German). Strassen und Verkehr 2000, Proceedings of the International Conference on Road and Traffic, 5: 53–58

Steffens, J. T., D. K. Heist, S. G. Perry, K. M. Zhang (2013): Modeling the effects of a solid barrier on pollutant dispersion under various atmospheric stability conditions. Atmospheric Environment, 69, 76-85.

Stocker, J., D. Heist, Ch. Hood, V. Isakov, D. Carruthers, S. Perry, M. Snyder, A. Venkatram, and S. Arunachalam (2013): Road Source Model Intercomparison Study using new and existing Datasets. Proceedings of the 15th Int. Conf. on Harmonisation within Atmospheric Dispersion Modelling for Regulatory Purposes, Madrid, Eds. (R. S. José and J. L. Pérez), 10-15.

US-EPA (2000): Meteorological Monitoring Guidance for Regulatory Modeling Applications. EPA-454/R-99-005. Office of Air and Radiation. Office of Air Quality Planning and Standards. Research Triangle Park, NC 27711, pp 171

VDI (2005): VDI Guideline 3783, Part 9, Environmental meteorology – Prognostic microscale wind field models – Evaluation for flow around buildings and obstacles. Commission of Air Pollution Prevention of VDI and DIN, Düsseldorf, Germany.

Venkatram, A., and S. Du (1997): An analysis of the asympototic behavior of cross-wind-integrated ground-level concentrations using Lagrangina Stochastic simulation. Atmos. Environ., 31, 1467-1476.